Effective parameters for periodic photonic structures of resonant elements

2009 J. Phys.: Condens. Matter 21 155404

(http://iopscience.iop.org/0953-8984/21/15/155404)

J. Phys.: Condens. Matter **21** (2009) 155404 (7pp) doi:10.1088/0953-8984/21/15/155404

Effective parameters for periodic photonic structures of resonant elements

C Tserkezis

Section of Solid State Physics, University of Athens, Panepistimioupolis, GR-157 84 Athens, Greece

E-mail: ctserk@phys.uoa.gr

Received 25 January 2009, in final form 17 February 2009
Published 20 March 2009
Online at stacks.iop.org/JPhysCM/21/155404

Abstract

We report on the effective electromagnetic parameters of metamaterials consisting of resonant building units, through systematic full-electrodynamic calculations by the layer-multiple-scattering method on a model system: a photonic crystal of metallic nanoshells. The results obtained by the *S*-matrix retrieval procedure for single- and multi-layer slabs of ordered arrays of such nanoshells are analysed in conjunction with the complex band structure of the corresponding infinite crystal and the Maxwell–Garnett effective-medium approximation. We discuss conditions that must be fulfilled in order for an effective-medium description of a metamaterial to be valid and explain artefacts which often occur in numerical calculations of the effective parameters. In particular, we propose a method to resolve ambiguities in the determination of the effective refractive index, which become prominent for thick slabs, based on the complex band structure of the infinite crystal.

(Some figures in this article are in colour only in the electronic version)

1. Introduction

The description of the electromagnetic (EM) response of a heterogeneous system through effective permittivity (ε_{eff}) and permeability (μ_{eff}) functions, i.e. the proper definition of an equivalent average homogeneous medium, has recently emerged as an important issue in relation to optical metamaterials [1–8]. The EM properties of a linear, passive system can be entirely specified by permittivity and permeability tensors that depend, in general, on the angular frequency ω and the wavevector $\mathbf{q}$. A heterogeneous system may consist, for example, of a periodic or random distribution of inclusions (scatterers) in an otherwise homogeneous host material; however, a periodic arrangement or patterning of scattering elements is more convenient from the point of view of design and analysis. If the wavelength of the EM field is much larger than the size of the scatterers and the distance between them, in order for a local description to be applicable, and if characterization of the system is restricted to one of its principal axes assuming a linearly polarized probing wave, only two scalar components, $\varepsilon_{\text{eff}}(\omega)$ and $\mu_{\text{eff}}(\omega)$, are relevant.

The most popular procedure for the assignment of effective material parameters to a heterogeneous medium consists of comparing the scattered waves in the far-field zone, i.e. the complex transmission and reflection coefficients (*S*-matrix elements) from a planar slab of the heterogeneous medium to those scattered from a slab of a hypothetical homogeneous material [1, 2, 7]. However, this technique often leads to nonphysical material parameters as a result of forcing a homogeneous material to reproduce *exactly* the features of the wave field scattered by the actual heterogeneous medium [9–12]. Such situations are typical, for example, for periodic photonic structures of resonant scatterers [9].

The present work reports on the effective material parameters of single- and multi-layer architectures of ordered arrays of metallic nanoshells, which exhibit tunable resonances. The results obtained by the *S*-matrix retrieval method are compared to those of the extended Maxwell–Garnett theory [13] and analysed in conjunction with relevant complex band-structure diagrams of the corresponding infinite crystal.

2. Method of calculation

Full-electrodynamic calculations for periodic structures of spherical particles of radius R consisting of a silica core ($\varepsilon_{\text{silica}} = 2.13$, $\mu_{\text{silica}} = 1$) of radius R_1 coated with a metallic shell of thickness D ($R = R_1 + D$) are carried out using the

on-shell layer-multiple-scattering method. This method was extensively presented elsewhere [14–17] and its suitability for photonic systems with absorptive and/or strongly dispersive constituents, such as metallic materials, was convincingly demonstrated [18–20]. Here we restrict ourselves to a brief description of the main points of the method.

The properties of the individual particles enter only through the corresponding scattering T matrix which, in the case under consideration, is evaluated using an efficient recursive formula for multiply coated spheres [21]. We assume that the metallic material is described by the simple Drude relative dielectric function [22]

$$\varepsilon_{\mathrm{m}} = 1 - \frac{\omega_{\mathrm{p}}^2}{\omega\left(\omega + \mathrm{i}\tau^{-1}\right)}, \tag{1}$$

where ω_{p} is the bulk plasma frequency, τ the relaxation time of the conduction band electrons that accounts for dissipative losses and $\mu_{\mathrm{m}} = 1$. For convenience, we shall express the angular frequency in units of ω_{p} and use c/ω_{p} as the length unit, where c is the velocity of light in vacuum. We note that, considering a typical value of 10 eV for $\hbar\omega_{\mathrm{p}}$, c/ω_{p} corresponds to about 20 nm.

Let us assume, to begin with, a two-dimensional (2D) periodic array of nanoshells on the xy plane and a plane EM wave incident on this layer. Because of the 2D periodicity of the structure, we write the component of the wavevector of the incident wave parallel to the layer, $\mathbf{q}_{\parallel}$, as $\mathbf{q}_{\parallel} = \mathbf{k}_{\parallel} + \mathbf{g}'$, where $\mathbf{k}_{\parallel}$, the reduced wavevector in the surface Brillouin zone (SBZ), is a conserved quantity in the scattering process and $\mathbf{g}'$ is a certain reciprocal vector of the given lattice. Therefore, the wavevector of the incident wave has the form $\mathbf{K}_{\mathbf{g}'}^{\pm} = \mathbf{k}_{\parallel} + \mathbf{g}' \pm [q^2 - (\mathbf{k}_{\parallel} + \mathbf{g}')^2]^{1/2}\,\hat{\mathbf{e}}_z$, where $\hat{\mathbf{e}}_z$ is the unit vector along the z axis and the $+$ or $-$ sign refers to incidence from the left ($z < 0$) or from the right ($z > 0$), i.e. a wave propagating towards the $z > 0$ or the $z < 0$ half-space, respectively. Since ω and $\mathbf{k}_{\parallel}$ are conserved quantities, the scattered field will consist of a series of plane waves with wavevectors

$$\mathbf{K}_{\mathbf{g}}^{\pm} = \mathbf{k}_{\parallel} + \mathbf{g} \pm \left[q^2 - \left(\mathbf{k}_{\parallel} + \mathbf{g}\right)^2\right]^{1/2} \hat{\mathbf{e}}_z, \qquad \forall\, \mathbf{g} \tag{2}$$

and polarizations along $\hat{\mathbf{e}}_1$ and $\hat{\mathbf{e}}_2$ (polar and azimuthal unit vectors, respectively, associated with every $\mathbf{K}_{\mathbf{g}}^{s}$, $s = \pm 1$). Though the scattered field consists, in general, of a number of diffracted beams corresponding to different 2D reciprocal lattice vectors $\mathbf{g}$, only beams for which $\mathbf{K}_{\mathbf{g}z}^{s}$ is real constitute propagating waves. When $(\mathbf{k}_{\parallel} + \mathbf{g})^2 > q^2$ the corresponding unit vectors $\hat{\mathbf{e}}_p$ become complex but they are still orthonormal ($\hat{\mathbf{e}}_p \cdot \hat{\mathbf{e}}_{p'} = \delta_{pp'}$, $p, p' = 1, 2$).

The scattering S matrix transforms the incident into the outgoing wave field (with all plane-wave components expanded about a common origin of coordinates). Explicit expressions for the matrix elements $S_{\mathbf{g}p;\mathbf{g}'p'}^{ss'}$ are summarized elsewhere [15, 16]. The S matrix of multi-layers with the same 2D periodicity is obtained by combining the corresponding transmission and reflection matrices of the component layers, with appropriate phase factors, in order to describe multiple scattering between the layers. The ratio of the transmitted or the reflected energy flux associated with the incident wave, on the right and the left of the slab, defines the transmittance, $\mathcal{T}(\omega, \mathbf{k}_{\parallel} + \mathbf{g}', p')$, or reflectance, $\mathcal{R}(\omega, \mathbf{k}_{\parallel} + \mathbf{g}', p')$, of the slab, respectively. On the other hand, for a three-dimensional (3D) crystal consisting of an infinite periodic sequence of layers along the z direction, applying the Bloch condition for the wave field in the region between two consecutive unit slabs leads to an eigenvalue equation, which gives the z component of the Bloch wavevector, k_z, for given ω and $\mathbf{k}_{\parallel}$ [15, 16].

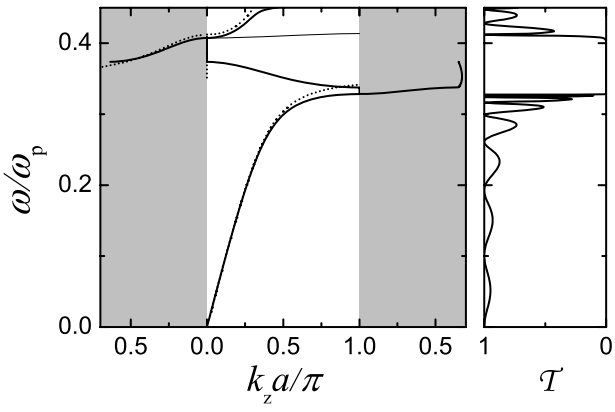

Figure 1. Left-hand diagram: the complex photonic band structure of a simple cubic crystal with lattice constant $a = 3c/\omega_{\mathrm{p}}$ of non-absorbing nanospheres consisting of a silica core of radius $R_1 = 0.7c/\omega_{\mathrm{p}}$ and a metallic shell of thickness $D = 0.3c/\omega_{\mathrm{p}}$, in air, along the [001] direction. The thick and thin lines denote doubly degenerate and non-degenerate bands, respectively. Over the gap region we display the doubly degenerate complex bands with the smallest in magnitude imaginary part (shown in the grey shaded areas). The dotted lines show the results of the Maxwell–Garnett effective-medium approximation. Right-hand diagram: transmittance at normal incidence of a slab of 8 (001) planes of the above crystal.

3. Complex band structure of a simple cubic crystal of metallic nanoshells

The spectra of plasmon modes in metallic nanoshells are much richer than those in solid metallic nanoparticles, since particle plasmons (at the outer surface of the shell) and cavity plasmons (at the inner surface of the shell), both of electric multipole type, can be concurrently excited. Moreover, the optical response of such nanoshells can be easily tuned by engineering their geometry. Plasmons of the outer and inner surfaces of the shell interact with each other and give rise to coupled resonant modes, one below the lower (particle-like) and one above the higher (cavity-like) plasmon modes [23, 24]. The interaction and the resulting level shifts increase as the overlap between the corresponding wave fields becomes larger, i.e. by reducing the shell thickness, and is more pronounced for the dipole modes because of their relatively larger spatial extent.

The photonic band structure of a simple cubic crystal, with lattice constant $a = 3c/\omega_{\mathrm{p}}$, of nanospheres consisting of a silica core ($R_1 = 0.7c/\omega_{\mathrm{p}}$) and a metallic shell ($D = 0.3c/\omega_{\mathrm{p}}$), in air, along the [001] direction, up to the frequency region of the dipole particle-like plasmon modes, is depicted in the left-hand diagram of figure 1. We note that the (001)

surface of the given crystal is a plane of mirror symmetry and, therefore, the frequency bands appear in pairs: $k_z(\omega, \mathbf{k}_\parallel)$ and $-k_z(\omega, \mathbf{k}_\parallel)$; for this reason, we show in the figure the bands only for positive k_z. We have deliberately disregarded absorption in the metallic material, taking $\tau^{-1} = 0$ in equation (1), in order to be able to interpret our results in an unambiguous manner. At low frequencies we obtain a doubly degenerate linear dispersion curve, as expected for propagation in a homogeneous medium characterized by a frequency-independent effective refractive index. This extended band interacts with the narrow doubly degenerate band which originates from the dipole particle-like plasmon modes of the individual nanoshells, weakly interacting between them. As a result, a frequency gap opens up about the crossing point of these bands and is referred to as a hybridization gap by analogy to the s–d hybridization gap in the electron band structure of transition metals [22]. In addition, there is a narrow non-degenerate band which is associated with collective dipole plasma oscillations along the propagation direction and, therefore, these modes cannot be excited by an externally incident (transverse) wave. In the gap region there are no propagating modes of the EM field and the real-frequency dispersion lines continue analytically in the complex k_z plane [25, 26]. There is, in principle, an infinite number of such complex bands but, over a gap region, it is the complex band of the appropriate symmetry (doubly degenerate in our case) with the smallest in magnitude imaginary part of k_z which determines the transmission of EM waves through a finite slab of the crystal, along the given direction. In the left-hand diagram of figure 1, in the gap, we show the real-frequency lines for complex eigenvalues k_z that correspond to the doubly degenerate complex bands with the smallest in magnitude imaginary part (plotted in the grey shaded areas). It can be seen that there are three segments of such complex bands in the gap region: one near the top of the gap, at the Brillouin zone centre, with $\mathrm{Re}\, k_z = 0$; one near the bottom of the gap, at the Brillouin zone edge, with $\mathrm{Re}\, k_z = \pi/a$; and one about the middle of the gap, with $0 \leqslant \mathrm{Re}\, k_z \leqslant \pi/a$.

The right-hand diagram of figure 1 displays the transmittance, $\mathcal{T}$, at normal incidence of a slab of the crystal consisting of $N_\mathrm{L} = 8$ (001) planes of nanoshells. The transmittance opposite the extended band exhibits the well-known Fabry–Perot oscillations due to multiple scattering between the surfaces of the slab. The period of these oscillations corresponds to $k_z a/\pi = 1/8$, as expected for the given thickness. In the gap region, the transmittance practically vanishes.

4. Maxwell–Garnett homogenization

It is interesting to examine whether the complex band structure shown in the left-hand diagram of figure 1 can correspond to a homogeneous effective medium. According to extended Maxwell–Garnett theories (see, e.g., [13] and references therein), such a medium can be defined by $\mu_\mathrm{eff} = 1$ and

$$\varepsilon_\mathrm{eff} = \frac{(qR)^3 - 3\mathrm{i} f T_{\mathrm{E1}}(\omega)}{(qR)^3 + \frac{3}{2}\mathrm{i} f T_{\mathrm{E1}}(\omega)}, \tag{3}$$

where f is the volume fraction occupied by the particles and T_{E1} is the electric dipole element of the T matrix. It is straightforward to show that, taking the long-wavelength limit of $T_{\mathrm{E1}}(\omega)$ given in [21], equation (3) reduces to a two-step Maxwell–Garnett approximation, where an effective permittivity ε_s is first obtained by homogenization of the individual coated particles:

$$\frac{\varepsilon_\mathrm{s} - \varepsilon_\mathrm{m}}{\varepsilon_\mathrm{s} + 2\varepsilon_\mathrm{m}} = \left(\frac{R_1}{R}\right)^3 \frac{\varepsilon_\mathrm{silica} - \varepsilon_\mathrm{m}}{\varepsilon_\mathrm{silica} + 2\varepsilon_\mathrm{m}} \tag{4}$$

and then ε_s is used to calculate ε_eff from

$$\frac{\varepsilon_\mathrm{eff} - 1}{\varepsilon_\mathrm{eff} + 2} = f\frac{\varepsilon_\mathrm{s} - 1}{\varepsilon_\mathrm{s} + 2}. \tag{5}$$

Using equations (4) and (5) we obtain an explicit expression for $\varepsilon_\mathrm{eff}(\omega)$, in terms of the dielectric functions of the constituent materials and the relevant volume filling fractions, which shows a resonant behaviour about the eigenfrequency of the dipole particle-like plasmon modes. Since there are no dissipative losses, ε_eff is real and exhibits an asymptotic variation taking negative values within a frequency interval next to the asymptote. In this region there can be no propagating modes of the EM field. We have there a frequency gap over which $k = \sqrt{\varepsilon_\mathrm{eff}\mu_\mathrm{eff}}\,\omega/c$ is purely imaginary ($\mathrm{Re}\, k = 0$). As can be seen in the corresponding band structure of the actual crystal (left-hand diagram of figure 1), the dominant evanescent modes near the top of the gap correspond, indeed, to $\mathrm{Re}\, k_z = 0$. Consequently, the form of the associated Bloch envelope wavefunctions ($\exp[-\mathrm{Im}\, k_z]$) is compatible with that of the evanescent modes supported in the Maxwell–Garnett effective medium, in the frequency region of negative ε_eff. In contrast, at lower frequencies within the gap, the dominant evanescent modes, resulting from destructive wave interference through multiple scattering in a periodic array of scatterers, corresponds to $\mathrm{Re}\, k_z \neq 0$ and such waves cannot be supported in the Maxwell–Garnett effective medium. On the other hand, as pointed out by Efros [11], to introduce macroscopic $\varepsilon_\mathrm{eff}(\omega)$ and $\mu_\mathrm{eff}(\omega)$, the wavelength inside the material must be much longer than the size of the unit cell. Therefore, this approximation for a photonic crystal becomes less accurate as the Bloch wavevector $\mathbf{k}$ approaches the Brillouin zone edges. This is shown in the left-hand diagram of figure 1, where the dispersion curves of the actual crystal are compared with those of the Maxwell–Garnett effective-medium approximation.

5. *S*-matrix retrieval of effective parameters

The *S*-matrix retrieval method defines the effective parameters based on the idea that a hypothetical homogeneous material plate, of thickness H, mimics an inhomogeneous slab in the sense that both systems produce the same outgoing field in the far zone, most usually for normal incidence. This does not mean that ε_eff and μ_eff describe the wave field inside the actual structure where, at a given frequency, it has the form of a Bloch wave rather than a simple plane wave. However, the effective parameters must be such that these two waves obey the same

dispersion relation and, therefore, have the same group (and phase) velocity. This remark is, of course, meaningful only if there is a single dominant relevant Bloch mode at the given frequency. Moreover, in order for an effective-medium description to be applicable, the wavelength in the embedding medium must be much larger than the in-plane period of the structure. This condition ensures that there is only a single propagating mode of the scattered EM field, for $\mathbf{g} = \mathbf{0}$ (see equation (2)), corresponding to outgoing waves (refracted and reflected beams). All other components of the wave field (diffracted beams) are evanescent. However, though restriction to the $\mathbf{g} = \mathbf{0}$ block of the S matrix is sufficient to obtain the scattered field by a finite slab of a given structure in the far zone, the full S matrix must be considered, in general, in order to describe interlayer coupling, which takes place through the near field in a multi-layer slab. On the other hand, since a (001) slab of the structure under consideration has a parallel plane of mirror symmetry and is polarization-insensitive at normal incidence, only two elements of the S matrix, $S^{++}_{\mathbf{01};\mathbf{01}}$ and $S^{+-}_{\mathbf{01};\mathbf{01}}$, are relevant and correspond to the transmission and reflection coefficients, t and r, respectively. In this case the S matrix has the simple form

$$\mathbf{S} = \begin{pmatrix} t & r \\ r & t \end{pmatrix} \tag{6}$$

and, since $\mathbf{S}$ is unitary because of flux conservation, its eigenvalues, $t + r$ and $t - r$, can be written as

$$t + r = \exp(\mathrm{i}2\delta_+) \qquad t - r = \exp(\mathrm{i}2\delta_-), \tag{7}$$

where δ_+, δ_-, the so-called scattering phase shifts, are real functions of frequency.

Inverting the standard Fresnel equations for an effective homogeneous slab described by a refractive index n_{eff} and an impedance z_{eff} in air, we find that, for normal incidence, the impedance and the refractive index of the slab can be retrieved through [1]

$$z_{\mathrm{eff}} = \pm\frac{\sqrt{(r-1)^2 - t^2}}{\sqrt{(r+1)^2 - t^2}} \tag{8}$$

and

$$\tan(\beta/2) = \pm\mathrm{i}\sqrt{\frac{r^2 - (1-t)^2}{r^2 - (1+t)^2}}, \tag{9}$$

respectively, where $\beta = (\omega/c)n_{\mathrm{eff}}H$. The sign of the impedance in equation (8) is determined by the condition $\mathrm{Re}\, z_{\mathrm{eff}} > 0$, required for a passive material. Moreover, in order to ensure an exponential decay of an outgoing wave, the imaginary part of the refractive index has to be positive, which fixes the sign in equation (9). With the help of equation (7), equations (8) and (9) lead to the following alternative expressions:

$$z_{\mathrm{eff}} = \pm\sqrt{\frac{\tan\delta_+}{\tan\delta_-}} \tag{10}$$

and

$$\tan(\beta/2) = \pm\mathrm{i}\sqrt{\tan\delta_+ \tan\delta_-}, \tag{11}$$

respectively. The effective permittivity and permeability of the slab are obtained from $\varepsilon_{\mathrm{eff}} = n_{\mathrm{eff}}/z_{\mathrm{eff}}$ and $\mu_{\mathrm{eff}} = n_{\mathrm{eff}}z_{\mathrm{eff}}$.

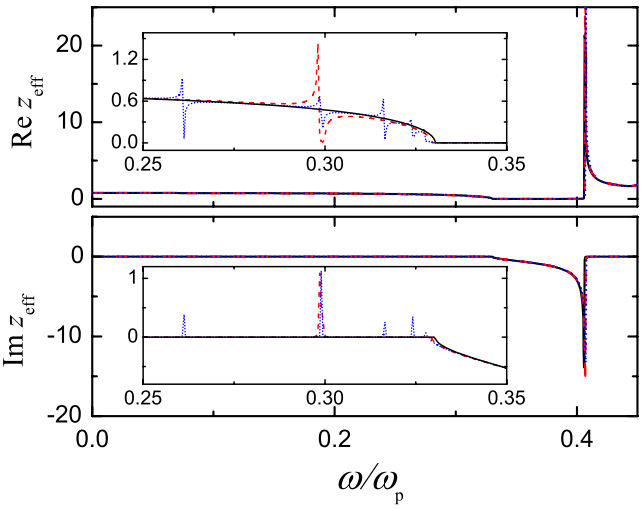

Figure 2. The real (upper diagram) and imaginary (lower diagram) parts of the effective impedance of one (black solid lines), two (red dashed lines) and eight (blue dotted lines) (001) layers of the photonic crystal under consideration, after elimination of the spurious sharp structures shown in the insets.

Since we view the simple cubic crystal under consideration as a sequence of N_{L} (001) planes, the boundary surfaces of each layer are at a distance $a/2$ from its centre, on the left and on the right of the plane of nanoshells, which corresponds to an effective layer thickness equal to a. In this way, the location of the two boundaries of an effective slab ensures a constant impedance for various slab thicknesses, $H = N_{\mathrm{L}}a$, as shown in figure 2. This is a necessary condition in order to be able to assign intrinsic values for $\varepsilon_{\mathrm{eff}}$ and μ_{eff} [1, 2]. It should be noted that the impedance, as calculated by equations (8) or (10), may exhibit spurious sharp structures about the Fabry–Perot resonance frequencies, ω_i, as shown in the insets to figure 2. These artefacts, which are multiplied by increasing the number of layers of the metamaterial slab, have also been noticed by others [2] but no clear explanation of their origin was given. We can understand the presence of these structures at the specific spectral positions as follows. At ω_i, $t = 1$ and $r = 0$ or, equivalently, $\tan\delta_+(\omega_i) = 0$ and $\tan\delta_-(\omega_i) = 0$. Therefore, in the vicinity of ω_i we can write $\tan\delta_+(\omega) \cong A_1(\omega - \omega_i) + A_2(\omega - \omega_i)^2$ and $\tan\delta_-(\omega) \cong B_1(\omega - \omega_i) + B_2(\omega - \omega_i)^2$, where A_1, A_2, B_1 and B_2 are appropriate expansion coefficients, and from equation (10) we obtain

$$z^2_{\mathrm{eff}} \cong \frac{A_1}{B_1} + \left(\frac{A_2}{B_1} - \frac{A_1B_2}{B_1^2}\right)(\omega - \omega_i), \tag{12}$$

i.e. z_{eff} varies smoothly with frequency about ω_i. However, in actual calculations, because of numerical inaccuracies, the roots of $\tan\delta_+(\omega)$ and $\tan\delta_-(\omega)$ may be slightly different, e.g. $\tan\delta_+(\omega_i + \Delta\omega_i) = 0$ and $\tan\delta_-(\omega_i) = 0$. As a result, in this case an additional singular term of order $1/(\omega - \omega_i)$ appears in the expansion of $z^2_{\mathrm{eff}}(\omega)$, about ω_i, which leads to an impedance function with sharp spurious structures, superimposed to a smooth background, as shown in the insets to figure 2.

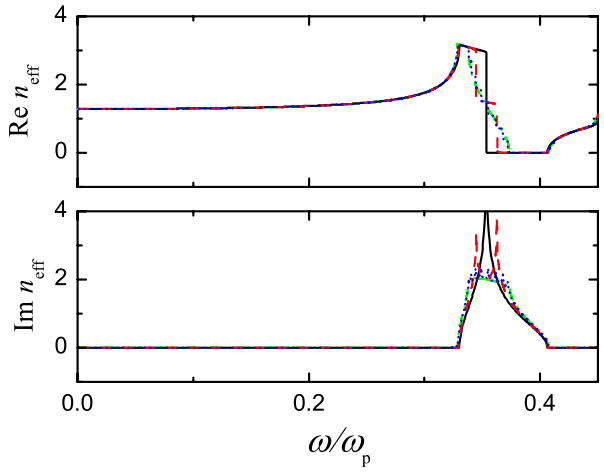

Figure 3. The real (upper diagram) and imaginary (lower diagram) parts of the effective refractive index of one (black solid lines), two (red dashed lines) and eight (blue dotted lines) (001) layers of the photonic crystal under consideration. The green dashed–dotted lines show the refractive index deduced from the corresponding complex band structure of the infinite crystal, shown in the left-hand diagram of figure 1.

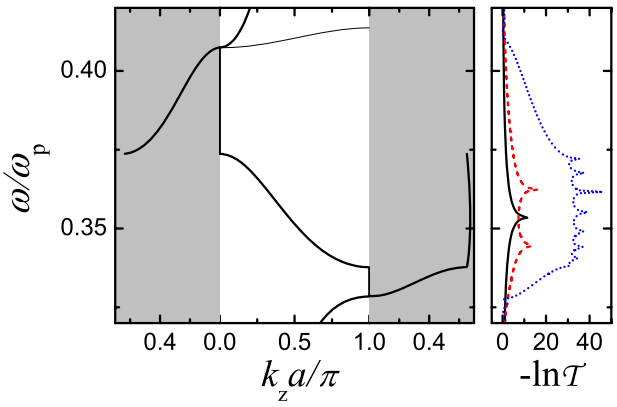

Figure 4. A detailed view of figure 1 about the region of the frequency gap. The (negative) natural logarithm of the transmittance of one (black solid lines), two (red dashed lines) and eight (blue dotted lines) layers is shown in the right-hand diagram.

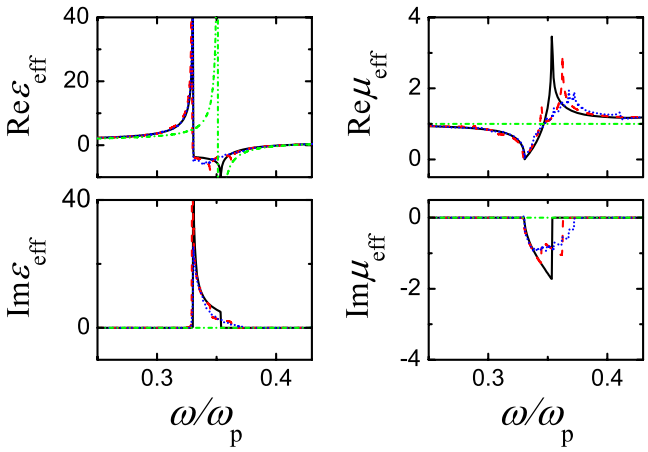

Figure 5. The real (upper diagrams) and imaginary (lower diagrams) parts of the permittivity (left-hand panel) and permeability (right-hand panel) of one (black solid lines), two (red dashed lines) and eight (blue dotted lines) layers of the photonic crystal under consideration. The green dashed-dotted lines show the results of the Maxwell–Garnett effective-medium approximation.

The effective refractive index often remains ambiguous because of the multiple branches of the tangent function appearing in equations (9) or (11). For a slab of small thickness, e.g. one monolayer, it is usually the fundamental branch which is relevant. However, for thicker slabs, higher branches may lie arbitrarily close to one another, making the selection of the correct branch difficult, as pointed out by others as well [1, 2, 29], while possible discontinuities due to resonances complicate the determination of an effective refractive index. Here we use the refractive index deduced from the complex band structure of the corresponding infinite crystal, $c[\mathrm{Re}\,k_z + \mathrm{i}\,\mathrm{Im}\,k_z]/\omega$, as a guide for choosing the proper branch, especially in the case of relatively thick slabs. In figure 3 we show $n_{\rm eff}$ of one, two and eight layers of the crystal under consideration, together with the refractive index deduced from the complex band structure of figure 1. It can be seen that very good convergence to the bulk results is obtained already at relatively thin slabs. Interestingly, in the gap region, $\mathrm{Re}\,n_{\rm eff}$ varies stairwise and corresponding peaks appear in $\mathrm{Im}\,n_{\rm eff}$, as many as the number of layers of the slab. These structures are associated with in-gap resonances of the slab [26]. In figure 4 we show the photonic band structure of figure 1 in more detail in the region of the frequency gap and the corresponding transmittance of one-, two-, and eight-layer thick slabs, in logarithmic scale. The resonances in the transmittance of a slab suggest that, at the corresponding frequencies, there exist resonances of some kind in the slab and we observe that such resonances appear within the frequency gap of the infinite crystal. These slab resonances are clearly due to resonances of the wave field localized on the individual nanoshells interacting very weakly between them. Of course, there cannot be states of the EM field in the infinite crystal within the gap; but in a slab of finite thickness, evanescent waves may exist and may lead to resonances of the EM field, with a high amplitude at the surfaces of the slab (within the nanoshells of the surface planes) and a much smaller amplitude in the middle of the slab (within the nanoshells of the middle planes). It is worth noting the fact that these resonances of the slab appear at frequencies along the real-frequency line corresponding to $\mathrm{Re}\,k_z a/\pi = \kappa/(N_{\rm L}+1)$, $\kappa = 1, 2, \ldots, N_{\rm L}$, where $N_{\rm L}$ is the number of layers in the slab. Since the S-matrix retrieval method defines the effective parameters so that the transmission spectrum is exactly reproduced, such in-gap resonances manifest themselves as discrete structures in the refractive index. As more layers are added to build the infinite crystal, these structures come closer to each other and become less sharp, leading to the smooth refractive index deduced from the corresponding complex band structure of the infinite crystal.

In figure 5 we present the effective permittivity, $\varepsilon_{\rm eff}$, and permeability, $\mu_{\rm eff}$, obtained from $z_{\rm eff}$ and $n_{\rm eff}$, for slabs one, two and eight layers thick. It can be seen that, although the building units of the structure are non-absorptive with purely

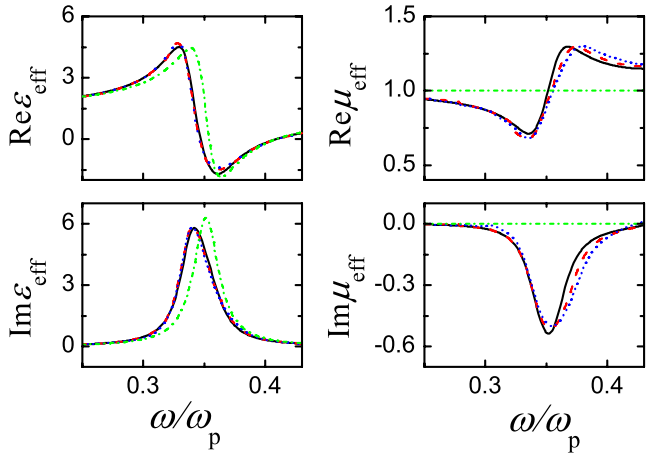

Figure 6. The real (upper diagrams) and imaginary (lower diagrams) parts of the permittivity (left-hand panel) and permeability (right-hand panel) of one (black solid lines), two (red dashed lines) and eight (blue dotted lines) layers of the photonic crystal under consideration, if absorptive losses in the metallic component are taken into account, by setting $\tau^{-1} = 0.025\omega_{\rm p}$ in equation (1). The green dashed–dotted lines show the results of the Maxwell–Garnett effective-medium approximation.

real permittivities and permeabilities, the *S*-matrix retrieval method leads to non-zero imaginary parts for both $\varepsilon_{\rm eff}$ and $\mu_{\rm eff}$ in the frequency region of the resonance. However, the retrieval procedure itself ensures that the values of $\varepsilon_{\rm eff}$ and $\mu_{\rm eff}$ are such that the absorption of each effective slab vanishes at any frequency. In some sense, it is not possible that the effective slab complies with the strong restriction to reproduce exactly the reflection and transmission coefficients of the actual metamaterial slab, with real functions $\varepsilon_{\rm eff}(\omega)$ and $\mu_{\rm eff}(\omega)$ in the resonance region. To make this possible, one has to assume complex functions with positive Im $\varepsilon_{\rm eff}$ and negative Im $\mu_{\rm eff}$, i.e. some fictitious losses which are counterbalanced by some fictitious gain. Obviously, this occurs for given slab thickness, specific characteristics of the incident field, etc, and, therefore, $\varepsilon_{\rm eff}$ and $\mu_{\rm eff}$ do not have the meaning of inherent material parameters.

So far we neglected absorptive losses. Although one may argue that a non-absorbing system is unphysical, such a system is useful for elucidating the underlying physics. Moreover, the effective parameters of a non-absorptive system provide a valuable guide for determining the effective parameters of a corresponding dissipative system. In figure 6 we present $\varepsilon_{\rm eff}$ and $\mu_{\rm eff}$ for the same slabs as in figure 5, if absorptive losses in the metallic component are taken into account by setting $\tau^{-1} = 0.025\omega_{\rm p}$ in equation (1). It can be seen that the effective parameters converge very fast with increasing slab thickness, while resonance structures become smoother and more extended in frequency, and sharp features are eliminated. It is worth noting that, even in the presence of absorption, the resonance in the effective permittivity is accompanied by a weak antiresonance in the effective permeability. Although such a behaviour has been observed and discussed by others as well [9, 27–29], it is further elucidated by our previous analysis for the ideal non-absorptive system (see figure 5).

6. Conclusion

In summary, we presented a theoretical study of the effective EM parameters of a photonic crystal of metallic nanoshells using the layer-multiple-scattering method. The results deduced by the *S*-matrix retrieval procedure for finite slabs of this crystal converge with increasing slab thickness and are consistent with the complex band structure of the infinite crystal. In this respect, our study establishes the complex photonic band structure as a new tool for the determination of the proper solution for the effective refractive index and its unambiguous calculation for arbitrarily thick metamaterial slabs [30, 31], even in regions of resonances. Moreover, we clarified the origin of peculiar spectral features and artefacts in the retrieved EM parameters, especially in regions of resonances, and discussed the meaning and limits of validity of these parameters, in conjunction with the Maxwell–Garnett effective-medium approximation.

Acknowledgment

This work was supported by the research programme ‘Kapodistrias’ of the University of Athens.

References

[1] Smith D R, Schultz S, Markoš P and Soukoulis C M 2002 *Phys. Rev.* B **65** 195104
[2] Chen X, Grzegorczyk T M, Wu B-I, Pacheco J Jr and Kong J A 2004 *Phys. Rev.* E **70** 016608
[3] Seetharamdoo D, Sauleau R, Mahdjoubi K and Tarot A-C 2005 *J. Appl. Phys.* **98** 063505
[4] Lerat J-M, Malléjac N and Acher O 2006 *J. Appl. Phys.* **100** 084908
[5] Silveirinha M G 2007 *Phys. Rev.* B **75** 115104
[6] Saenz E, Ikonen P M T, Gonzalo R and Tretyakov S A 2007 *J. Appl. Phys.* **101** 114910
[7] Menzel C, Rockstuhl C, Paul T, Lederer F and Pertsch T 2008 *Phys. Rev.* B **77** 195328
[8] Śmigaj W and Gralak B 2008 *Phys. Rev.* B **77** 235445
[9] Koschny Th, Markoš P, Smith D R and Soukoulis C M 2003 *Phys. Rev.* E **68** 065602(R)
[10] Depine R A and Lahtakia A 2004 *Phys. Rev.* E **70** 048601
[11] Efros A L 2004 *Phys. Rev.* E **70** 048602
[12] Koschny Th, Markoš P, Economou E N, Smith D R, Vier D C and Soukoulis C M 2005 *Phys. Rev.* B **71** 245105
[13] Ruppin R 2000 *Opt. Commun.* **182** 273
[14] Stefanou N and Modinos A 1991 *J. Phys.: Condens. Matter* **3** 8135
[15] Stefanou N, Yannopapas V and Modinos A 1998 *Comput. Phys. Commun.* **113** 49
[16] Stefanou N, Yannopapas V and Modinos A 2000 *Comput. Phys. Commun.* **132** 189
[17] Gantzounis G and Stefanou N 2006 *Phys. Rev.* B **73** 035115
[18] Stefanou N and Modinos A 1991 *J. Phys.: Condens. Matter* **3** 8149
[19] Stefanou N, Modinos A and Yannopapas V 2001 *Solid State Commun.* **118** 69
[20] Modinos A, Stefanou N and Yannopapas V 2001 *Opt. Express* **8** 197
[21] Stefanou N, Tserkezis C and Gantzounis G 2008 *Proc. SPIE* **6989** 698910
[22] Ashcroft N W and Mermin N D 1976 *Solid State Physics* (New York: Saunders)

[23] Prodan E, Radloff C, Halas N J and Nordlander P 2003 *Science* **302** 419
[24] Teperik T V, Popov V V and García de Abajo F J 2004 *Phys. Rev.* B **69** 155402
[25] Heine V 1963 *Proc. Phys. Soc.* **81** 300
[26] Gantzounis G and Stefanou N 2005 *Phys. Rev.* B **72** 075107
[27] Lidorikis E, Egusa S and Joannopoulos J D 2007 *J. Appl. Phys.* **101** 054304
[28] O'Brien S and Pendry J B 2002 *J. Phys.: Condens. Matter* **14** 4035
[29] Smith D R, Vier D C, Koschny Th and Soukoulis C M 2005 *Phys. Rev.* E **71** 036617
[30] Zhang S, Fan W, Panoiu N C, Malloy K J, Osgood R M and Brueck S R J 2006 *Opt. Express* **14** 6778
[31] Rockstuhl C, Paul T, Lederer F, Pertsch T, Zentgraf T, Meyrath T P and Giessen H 2008 *Phys. Rev.* B **77** 035126